JOURNAL OF THERMOPHYSICS AND HEAT TRANSFER
Vol. 21, No. 3, July–September 2007

Rib Spacing Effect on Heat Transfer in Rotating Two-Pass Ribbed Channel ($AR = 1{:}2$)

Yao-Hsien Liu*
Texas A&M University, College Station, Texas 77843-3123
Lesley M. Wright†
University of Arizona, Tuscon, Arizona 85721-0119
Wen-Lung Fu‡
MiTAC International Corporation, Hsinchu 300, Taiwan, Republic of China
and
Je-Chin Han§
Texas A&M University, College Station, Texas 77843-3123

DOI: 10.2514/1.29128

Rib turbulators are commonly used to enhance the heat transfer within internal cooling passages of advanced gas turbine blades. Many factors affect the thermal performance of a cooling channel with ribs. This study experimentally investigates the effect of rib spacing on the heat transfer enhancement, pressure penalty, and thus the overall thermal performance in both rotating and nonrotating rectangular, cooling channels. In the 1:2 rectangular channels, 45 deg angled ribs are placed on the leading and trailing surfaces. The pitch of the ribs varies, so rib pitch-to-height (P/e) ratios of 10, 7.5, 5, and 3 are considered. Square ribs with a 1.59 mm × 1.59 mm cross section are used for all rib spacing, so the height-to-hydraulic diameter (e/D_h) ratio remains constant at 0.094. With a constant rotational speed of 550 rpm and the Reynolds number ranging from 5000 to 40,000, the rotation number in turn varies from 0.2 to 0.02. Because the skewed turbulators induce secondary flow along the length of the rib, the very close rib spacing of $P/e = 3$ has the best thermal performance in both rotating and nonrotating channels. This close spacing yields the greatest heat transfer enhancement, whereas the $P/e = 5$ spacing has the greatest pressure penalty. In addition, the effect of rotation is more pronounced in the channel with the rib spacing of 3. As more ribs are added, the channel is approaching a smooth channel, and the strength of the rotation induced vortices increases.

Nomenclature

A_{smooth}	=	area of the smooth copper plate
A_{total}	=	area of the smooth copper plate and the ribs
AR	=	channel aspect ratio, $W{:}H$
Bo_x	=	local buoyancy parameter
D_h	=	channel hydraulic diameter
e	=	rib height
f	=	friction factor
f_0	=	fully developed friction factor in nonrotating, smooth pipe
H	=	channel height
h	=	regionally averaged heat transfer coefficient
k	=	thermal conductivity of the coolant
L	=	length of the rib-roughened portion of the test section
Nu	=	regionally averaged Nusselt number
Nu_0	=	Nusselt number of the fully developed turbulent flow in nonrotating smooth pipe
P	=	rib spacing
P_i	=	pressure at the inlet of the test section
P_o	=	pressure at the outlet of the test section
Pr	=	Prandtl number of the coolant
q''_{loss}	=	heat loss through the wall
q''_w	=	heat flux at the wall
Re	=	Reynolds number, $\rho V D_h/\mu$
Ro	=	rotation number, $\Omega D_h/V$
R_x	=	local radius of rotation
$T_{b,x}$	=	local coolant bulk temperature
$T_{f,x}$	=	local film temperature ($=(T_{w,x} + T_{b,x})/2$)
$T_{w,x}$	=	local wall temperature
V	=	bulk velocity in streamwise direction
W	=	channel width
α	=	rib angle of attack
β	=	angle of channel orientation with respect to the axis of rotation
$(\Delta\rho/\rho)_x$	=	local coolant-to-wall density ratio $[=(T_{w,x} - T_{b,x})/T_{f,x}]$
η	=	thermal performance
μ	=	viscosity of the coolant
ρ	=	density of the coolant
Ω	=	rotational speed

Received 2 December 2006; revision received 8 February 2007; accepted for publication 9 February 2007.

*Research Assistant, Department of Mechanical Engineering.
†Assistant Professor, Department of Aerospace and Mechanical Engineering.
‡Senior Thermal Engineer.
§Distinguished Professor and M. C. Easterling Chair Professor, Turbine Heat Transfer Laboratory, Department of Mechanical Engineering; jc-han@tamu.edu. Associate Fellow AIAA.

Introduction

GAS turbine engines are a common sight in the world's industrialized society. With the growing world economy, they are commonly used by the utility industry for land based power generation, and the engines are relied on heavily for marine and aircraft propulsion. With gas turbines used in such a variety of applications, it is vital that the engines operate efficiently, without premature failure. The thermal efficiency of the engine can be improved by raising the turbine inlet temperature. However, raising the temperature beyond the melting point of the metal components can result in component failure, leading to engine failure. The turbine components can survive these extreme conditions, if they are

properly protected and/or cooled. A thermal barrier coating (TBC) may be applied to the outer surface of the turbine blades and vanes to add an insulating layer of protection between the hot mainstream gas and the metallic airfoils.

In addition to protecting the airfoils, a variety of cooling techniques can be used to remove heat from the blades and vanes. *Gas Turbine Heat Transfer and Cooling Technology* [1] is a resource that reviews many techniques that have been studied to cool the turbine blades and vanes. Cooling air is extracted from the engine's compressor and circulated through various cooling passages within the blade. In the leading edge region of the airfoils, aggressive cooling techniques are needed to alleviate the extremely high heat load developed due to stagnation of the mainstream flow. To enhance heat transfer within the other cooling channels, rib turbulators or pin fins may be cast on the walls of the channel, as shown in Fig. 1. Although other methods can be used to enhance the heat transferred from the blade wall to the cooling air, rib turbulated cooling is the most widely used internal cooling technique.

Many factors affect the level of heat transfer enhancement in ribbed channels. The rib configuration has the most profound impact on the flow through the channel and therefore, the level of heat transfer enhancement. However, many factors come together to form a single rib configuration; these factors include, but are not limited to rib orientation (angle of attack), rib spacing (P/e), rib height (e/D_h), and rib cross section (square, sharp corners, rounded corners, etc.). These factors, coupled with a wide range of channel sizes (aspect ratios), can result in very different levels of heat transfer enhancement through the cooling channels.

With so many factors that require consideration, significant resources have been directed to understanding flow and heat transfer in rib-roughened channels. Fundamental studies began in nonrotating cooling channels with rib turbulators. As shown in Fig. 1, the cross section of the cooling channels varies from the leading edge to the trailing edge of the blade. The flow through these channels varies and results in different levels of heat transfer enhancement for different channels. Several investigations with various channel aspect ratios ($AR = 1{:}4, 1{:}2, 1{:}1, 2{:}1$, and $4{:}1$) have been completed by Han and Park [2] and Park et al. [3]. They tested the 30, 45, 60, and 90 deg angled ribs. The results suggested that the low aspect ratio channels ($W/H < 1$) can give better heat transfer performance than

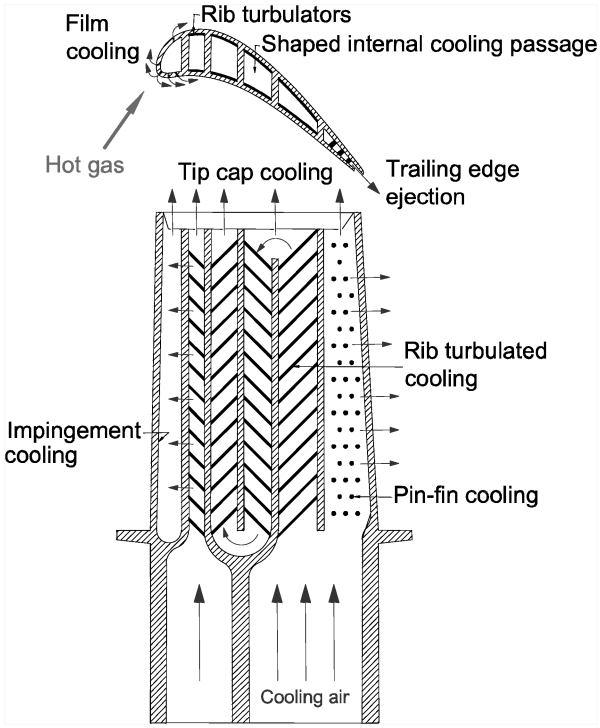

Fig. 1 Common internal cooling techniques applied to advanced turbine blades.

the high aspect ratio channels ($W/H > 1$). Park et al. [3] also combined the effect of channel aspect ratio with various angled ribs. The result showed that the ribs with 60/45 deg angle of attack have a higher heat transfer coefficient in the square channel. For low aspect ratio channels ($AR = 1{:}2$ and $1{:}4$), the 45/60 deg angled ribs provide better heat transfer performance while the 30/45 deg angled ribs are better for high aspect ratio channels ($AR = 2{:}1$ and $4{:}1$).

The rib spacing also has a profound impact on the heat transfer enhancement in rib-roughened channels. The space between the ribs will change the flow reattachment pattern and create different heat transfer results. Han et al. [4] investigated the rib spacing effects in a high aspect ratio channel ($AR = 12{:}1$). Heat transfer and pressure drop were measured for several different P/e ratios (5, 7.5, 10, 15, and 20). The result showed that the highest heat transfer occurred at $P/e = 10$ for orthogonal ribs. Han [5] tested the rib spacing effects for $P/e = 10$, 20, and 40 in a square channel. He found that both the average friction factor and the Stanton number decreased with increasing P/e. Han [6] also extended this study to include rectangular channels. The P/e ratios tested were 10 and 20, and five different channels were tested ($AR = 1{:}4, 1{:}2, 1{:}1, 2{:}1$, and $4{:}1$). The results also showed that $P/e = 10$ produced the highest heat transfer in all aspect ratio channels considered. Taslim and Wadsworth [7] measured the rib surface-averaged heat transfer coefficient for orthogonal ribs in a square channel. The P/e ratios tested were 5, 7.5, 8.5, and 10. They concluded that for the sharp-edge ribs, $P/e = 8.5$ produced the highest heat transfer coefficient (which is comparable to the findings of Han et al. [2–6].

Taslim and Lengkong [8] extended the study to 45 deg staggered square ribs in a square channel. The rib spacing-to-height ratios were 5, 8.5, and 10, and the height-to-passage hydraulic diameter ratios were 0.133, 0.167, and 0.25. They concluded that the thermal performance decreased as the blockage ratio increases due to the increased frictional losses. For the 45 deg angled ribs in the staggered arrangement, the case for $P/e = 10$ and $e/D_h = 0.133$ had the best thermal performance. Taslim and Korotky [9] investigated the rib spacing effects for nonsquare ribs in a square channel. The rib spacing-to-height ratios (P/e) were 5, 8.5, and 10, and the height-to-passage hydraulic diameter ratios (e/D_h) were 0.133, 0.167, and 0.25. They concluded that for the low blockage ratios ($e/D_h = 0.133$ and 0.167), the results of $P/e = 10$ have the highest heat transfer coefficient. For the high-blockage-ratio ($e/D_h = 0.25$) ribs, the results for heat transfer were insensitive to the P/e ratio. Rau et al. [10] used liquid crystals to measure the heat transfer coefficients and laser Doppler velocimetry (LDV) to measure the flowfield in a square channel. Orthogonal ribs with $e/D_h = 0.1$ were studied at three spacings: $P/e = 6$, 9, and 12. The results indicated that the average heat transfer enhancement on the floor (between the ribs) gave a maximum value for $P/e = 9$. Astarita and Cardone [11] used infrared (IR) thermography with the heated-thin-foil technique to investigate the rib spacing effects in a square channel. The ribs tested were 30 and 45 deg angled ribs, and $P/e = 10$ and 20. They concluded that the Nusselt number ratio for $P/e = 20$ is lower than $P/e = 10$. The reason is that fewer ribs induced lower overall turbulence, and with fewer instances of separation and reattachment, a thicker boundary layer resulted in decreased heat transfer.

Not only is the heat transfer enhancement influenced by the rib spacing, it is also affected by the rib height. Taslim and Spring [12] used a liquid crystal technique to study the effects of rib profile, spacing, and blockage on the heat transfer coefficients in two rectangular channels with $AR = 0.5$ and 0.55. They found that the sensitivity of the Nusselt number on P/e decreases as e/D_h increases. Bailey and Bunker [13] also investigated the rib blockage effects using liquid crystal in a rectangular channel with $AR = 1{:}2.5$. They found that higher-blockage ribs with a 45 deg angle of attack gave lower friction factors compared to the 90 deg angled ribs.

Experiments with rotation have been conducted to more closely model engine cooling environments. The interaction of the secondary flow induced by rotation and the rib turbulators results in different heat transfer trends, as in the stationary channels. Wagner et al. [14,15] conducted a detailed experimental study to determine the effects of rotation (buoyancy and Coriolis forces) on the local

heat transfer of a multipass square channel with smooth walls. They concluded that the first pass of the coolant passage with rotation created a thinner boundary layer on the trailing surface and a thicker boundary layer on the leading surface resulting in increased heat transfer and decreased heat transfer, respectively. The leading surface Nusselt number ratios in the second pass were higher than the trailing surface Nusselt number ratios because of the reversal of the Coriolis force direction.

Johnson et al. [16] used their square channel to measure the heat transfer coefficients in channels with 45 deg angled ribs. Similar to their smooth channels, the leading and trailing surfaces of the channel experienced different levels of heat transfer enhancement. However, because the rib turbulators increase the heat transfer from the channel walls, the difference between the leading and trailing ribbed walls is less than the difference between the smooth walls. Similar results have been observed in square channels with angled ribs by Dutta and Han .

Similar to nonrotating channels, the heat transfer enhancement in ribbed channels has been studied in a wide range of aspect ratio channels. Al-Hadhrami and Han [18] and Fu et al. [19] investigated the heat transfer enhancement in 2:1 channels with rib turbulators. The more narrow 4:1 channels with rib turbulators have been the focus of several studies [20,21]. With these channels having relatively wide leading and trailing surfaces, both studies recorded significant spanwise variation in the heat transfer coefficients on both the leading and trailing surfaces. The effect of rotation on the heat transfer coefficients in channels located near the leading edge of the blade has also been reported. The effect of rotation is more significant in these channels with low aspect ratios than in channels with high aspect ratios [22]. When the aspect ratio is reduced to 1:2 and 1:4, Fu et al. [22] showed that the combination of the rib and rotation induced secondary flows can adversely affect the heat transfer from the first-pass leading surface.

The e/D_h effects under the rotating condition have been studied by Taslim et al. [23,24]. The liquid crystal technique was used to measure the heat transfer coefficient for different rib heights under the rotating condition. The blockage ratios they studied were 0.1333, 0.25, and 0.3333 in the channels with aspect ratios of 1:1 and 2:1. The results showed that for the high channel aspect ratio and the low rib blockage ratio, there was a steady increase in the heat transfer coefficient on the trailing side as the rotating number increases. A steady decrease in heat transfer coefficient on the leading side with the rotation number was also observed.

Rib turbulator studies began in square channels with orthogonal ribs and were quickly extended to include skewed ribs in channels of various cross sections. Many studies agreed that the optimum rib spacing for square channels with 90 deg ribs is approximately equal to 10 times the rib height ($P/e = 10$). Although this finding has been extended to include rectangular channels, conclusive results have not been reported for channels with skewed ribs, especially 45 deg angled ribs. Furthermore, the optimum spacing found in stationary channels has been applied to rotating channels by many groups, but the spacing yielding the greatest heat transfer enhancement may vary from stationary to rotating channels.

The objective of the current study is to extend the previous work that has been conducted in both stationary and rotating cooling channels with angled ribs. Although many groups have focused their resources to study heat transfer in rotating channels, most of the experimental data covers square or high aspect ratio channels ($AR \geq 1$). The data that are available for 1:2 channels show that the effect of rotation can adversely affect the level of heat transfer, including in rib-roughened channels, especially on the first-pass leading surface. It is vital to confirm this finding, so that reliable data are available for turbine designers. In addition, it is necessary to determine the rib spacing that yields the best thermal performance in rotating, rectangular cooling channels with an aspect ratio of 1:2. This includes determining which rib spacing ($P/e = 3$, 5, 7.5, and 10) generates the greatest heat transfer enhancement and the least frictional losses in the two-pass rotating channel. In addition, the heat transfer coefficients, pressure losses, and thermal performance are measured in nonrotating channels to determine if previous findings for nonrotating channels with orthogonal ribs can be extended to rectangular rotating cooling channels. Finally, it is important to consider the effect of the heat transfer area on the heat transfer enhancement. One advantage of adding rib turbulators to the cooling channel is that the heat transfer area is increased. For large rib spacing, this area increase may not be significant; however, for closely spaced ribs, the area increased by the ribs can be significant. Therefore, this study will attempt to clarify the difference in the heat transfer coefficients calculated using the smooth channel area and the total heat transfer area (including the surface of the ribs).

Test Facility

The test rig shown in Fig. 2 was used to conduct both nonrotating and rotating experimental turbine blade cooling studies. This rig, previously used by Fu et al. [22] and validated for the previous study, consists of a variable frequency motor connected to a vertical, hollow, rotating shaft. This shaft runs from the base of the test rig to a hollow arm that is attached orthogonally to the rotating shaft. This hollow arm houses the experimental test section. Cooling air travels through an American Society of Mechanical Engineers (ASME) square edge orifice meter, through the vertical shaft, turns 90 deg into the rotating arm, into the serpentine test section, and finally is expelled to the room. Power is supplied to the heaters placed within the test section and thermocouple signals from the test section are transmitted to a computer with National Instruments' data acquisition software, Lab View, via a 100-channel slip ring placed above the rotating arm. In addition, a 48-channel Scanivalve pressure transducer is located along the axis of rotation atop the slip ring. Voltage signals from the pressure transducer are also transmitted through the slip ring to Lab View.

Figure 3 shows a layout of the 1:2 test section used in the current study. The 1:2 test section is 12.7×25.4 mm in cross section with a hydraulic diameter (D_h) of 16.93 mm. The test section contains a 222.25 mm unheated entrance length to provide a hydrodynamic fully developed flow condition. Each pass has a 152.4 mm long heating section. The clearance of the 180 deg sharp turn is 12.7 mm from tip to end wall. The divider wall has a thickness of 12.7 mm with a 6.35 mm radius at the tip. Cooling air is expelled to the atmosphere through a 6.35 mm radius hole in the second pass. The distance from the end of the heated section in the second pass to the exit hole is 152.4 mm.

As shown in Fig. 3, each pass is divided into six segments. Each segment contains six copper plates: one for the leading, one for the trailing, two for the outer, and two for the inner walls. The inner wall

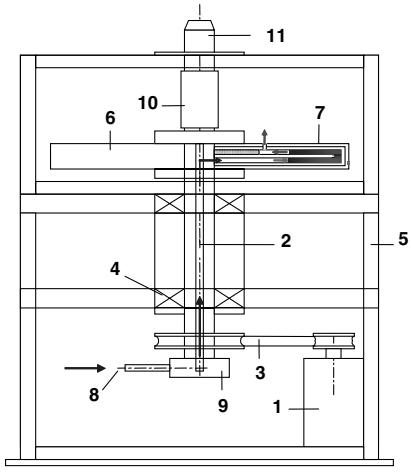

1. Electrical Motor with Controller
2. Rotating Shaft
3. Belt Drive Pulley System
4. Bearing Support System
5. Steel Table
6. Rotating Arm
7. Test Section
8. Compressor Air
9. Rotary Seal
10. Slip Ring
11. Scanivalve Pressure Transducer

Fig. 2 Schematic of the test facility.

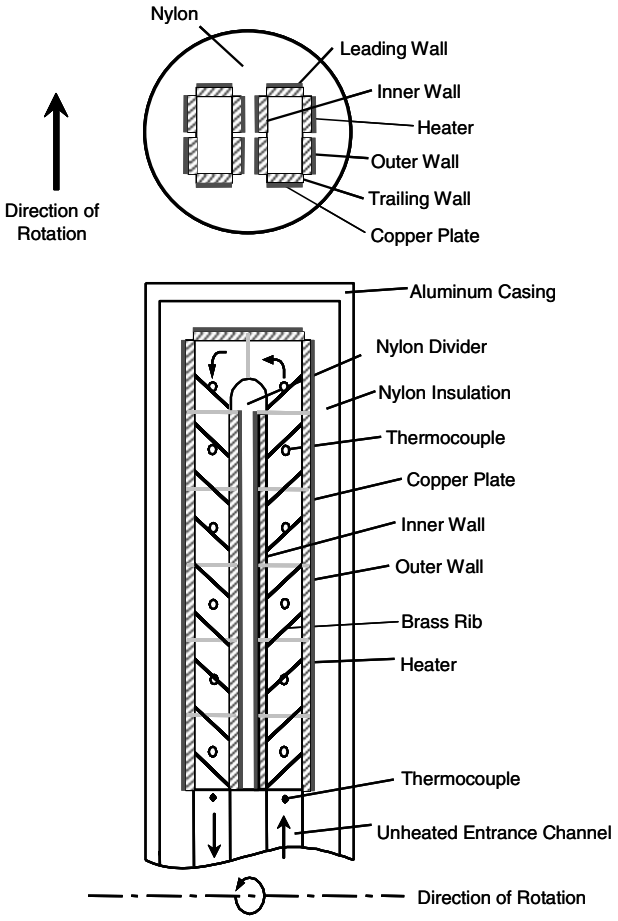

Fig. 3 Cross sectional view of the 1:2 test section.

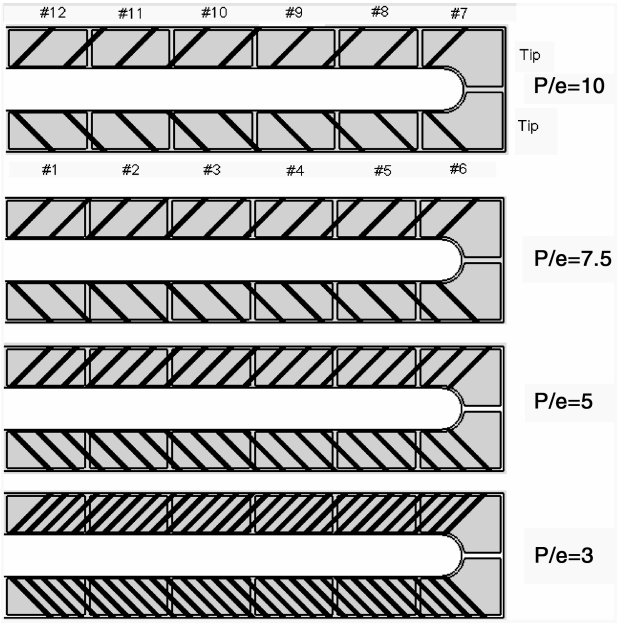

Fig. 4 Rib spacings considered in the present study.

has only five segments in the flow direction because of the 180 deg turn. The copper plates, each of which is $11.11 \times 23.81 \times 3.18$ mm^3 thick, are mounted in a nylon substrate, which comprises the bulk of the test section. Prefabricated flexible heaters are installed beneath the copper plates. A total of 13 heaters are used for the test section. All heaters supply steady, uniform heat flux to the copper plates. Sufficient power is supplied to maintain a maximum wall temperature of nearly 65°C for the corresponding section. This corresponds to an inlet coolant-to-wall density (temperature) ratio of 0.115 for every test. Thermal conducting paste is applied between the heater and the copper plates to promote heat transfer from the heater to the plates. Each 3.18 mm thick copper plate has a 1.59 mm deep blind hole drilled in the backside in which a copper–constantan thermocouple is installed 1.59 mm from the plate surface with thermal conducting glue. Thin nylon strips (1.59 mm) between the copper plates reduce the conduction effect between the plates. With the high conductivity copper plates, the temperature measured by each thermocouple represents the temperature throughout the entire copper plate. This uniform temperature assumption has been validated by the calculation of the Biot number for each copper plate. For all copper plates, the calculated Biot number is less than 0.1, which indicates spatial temperature uniformity throughout the copper plate. Therefore, each thermocouple gives a regional temperature measurement.

To account for frictional losses in the channel, the pressure at the inlet and outlet of the channel is measured, so the pressure drop could be easily calculated. Two pressure taps are located at the inlet of the heated portion of the test section, and two pressure taps are located at the end of the heated test section (all pressure taps are located on the outer walls of the test section). Hoses connect the pressure taps to the Scanivalve pressure transducer, and the voltage signal is converted to a gauge pressure based on a calibration relating a known pressure to a measured voltage. All pressure loss measurements are completed in the absence of heating. The assembled test section fits snugly into the rotating arm. The arm rotates at a constant speed of 550 rpm. The Reynolds number ranges from 5000 to 40,000, and the rotation number ranges from 0.026 to 0.2. The rib turbulators used in the present study are made of brass and have a 1.59×1.59 mm^2 square cross section. They are attached to both the leading and trailing surfaces, so the ribs on these surfaces are parallel. They are attached to the surfaces using a thin layer of conductive glue, so the thermal resistance between the copper plates and ribs is minimized. The ribs are skewed, so the angle of attack is 45 deg. Because this objective focuses on the effect of rib spacing, four different rib pitch-to-height ratios are studied: $P/e = 10$, 7.5, 5, and 3. Figure 4 shows that the number of ribs placed on the channel wall varies from 18 ($P/e = 10$) to 58 ($P/e = 3$). Therefore, the pitch of the ribs varies from 15.88 mm ($P/e = 10$) to 4.76 mm ($P/e = 3$).

Data Reduction

Heat Transfer Measurement

The purpose of the research is to investigate the regionally averaged heat transfer coefficient in the rectangular channels with rib-roughened walls. By measuring the temperature of each copper plate and the energy supplied by the heater, we can get the regionally averaged heat transfer coefficient of each copper plate. The regional heat transfer coefficient can be calculated from

$$h = \frac{q''_w - q''_{\text{loss}}}{T_{w,x} - T_{b,x}} \tag{1}$$

$T_{w,x}$ is the wall temperature measured by the thermocouple, and $T_{b,x}$ is the bulk temperature calculated from linear interpolation between the inlet temperature and the outlet temperature. Therefore, the bulk temperature at any location in the test section can be calculated using linear interpolation. However, the local bulk temperature can also be calculated using the conservation of energy principle. For the present study, both methods compare very well; the difference between the two methods is less than 5%. The heat flux from the heater q''_w is calculated from the product of the voltage and current (V^*I) supplied to the heater from a variable transformer divided by the applicable heat transfer area. The heat loss will come from conduction through the nylon test section. The heat losses are determined under a no flow condition, with fiberglass insulation in the channel to prevent natural convection within the channel.

The heat flux is calculated based on the copper plate area (A_{smooth}) and the area including the copper plate and the ribs (A_{total}). Calculating the heat transfer coefficient based on the smooth channel

Table 1 Ratios of the area increase by the ribs in the channel

P/e	Area increased
10	26.47%
7.5	35.29%
5	52.94%
3	88.24%

area shows the true heat transfer enhancement compared to a nonrotating, smooth channel. If the heat transfer coefficients are calculated based on the total area (the area between two ribs plus three sides of the ribs), the advantage of the additional area is eliminated. But this gives a true value for the heat transfer coefficients within the channel. The heat transfer coefficients based on these two areas are obtained and discussed. As shown in Table 1, when the pitch-to-height ratio is lowered to 3, the heat transfer area increases by more than 88% (as compared to the smooth channel area), whereas with the more traditional spacing of $P/e = 10$, the area increases 26.5%. From the heat transfer coefficient, we can get the Nusselt number. The Dittus-Boelter/McAdams correlation is used to calculate the Nusselt number for the fully developed turbulent flow through a smooth circular tube. The Nusselt number ratio Nu/Nu_0 can be obtained

$$\frac{Nu}{Nu_0} = \frac{hD_h}{k}\frac{1}{0.023Re^{0.8}Pr^{0.4}} \tag{2}$$

All air properties are taken based on the bulk air temperature with a Prandtl number of 0.71.

Friction Factor Measurement

To measure the friction factor, the pressure difference between the inlet and the outlet must be obtained. The friction factor can be calculated from the pressure drop between the inlet and the outlet of the channel.

$$f = (P_i - P_o)\Big/4\left(\frac{L}{D_h}\right)\frac{1}{2}\rho V^2 \tag{3}$$

The inlet pressure P_i is taken as the average of the two pressure measurements at the channel entrance, and the outlet pressure P_e is the average of the two outlet pressure measurements.

The frictional losses can then be calculated by dividing the friction factor by the turbulent friction factor in a smooth tube as given by the Blasius equation. With the friction factor in a smooth tube defined in Eq. (4), the friction factor ratio can be expressed in terms of the measured friction factor, and the smooth channel friction factor, as shown in Eq. (5).

$$f_0 = 0.079Re^{-0.25} \tag{4}$$

$$f/f_0 = f/0.079Re^{-0.25} \tag{5}$$

Thermal Performance

Based on the heat transfer enhancement (Nu/Nu_0) and the frictional loss penalty (f/f_0), the thermal performance (η) for a given rib spacing can be calculated. Equation (6) shows the thermal performance based on the constant pumping power condition:

$$\eta = (Nu/Nu_0)/(f/f_0)^{1/3} \tag{6}$$

An uncertainty analysis was performed based on the method from Kline and McClintock [25]. The uncertainty from the thermocouple is about 0.5°C. The uncertainty for the Nusselt number ratio is approximately 7% for the highest Reynolds number and the maximum uncertainty is approximately 21% from the low heat flux wall for the lowest Reynolds number of the rotating cooling channel. The maximum uncertainty for the pressure measurement is 7% at $Re = 10,000$ and drops to 3% at $Re = 40,000$.

Results and Discussion

Secondary Flow Behavior

Before discussing the experimental results for the two-pass cooling channels with angled ribs, it is necessary to understand the flow behavior of the coolant inside the channel. As described previously, the orientation of the rib turbulators has a significant impact on the level of heat transfer enhancement. Skewed ribs yield significantly higher heat transfer enhancement than orthogonal ribs. This is due to the secondary flow induced by the angled ribs. Rib turbulators are also widely known as "trip strips" as they simply trip the developing boundary layer in the internal channel. After the boundary layer is disturbed, redevelopment begins, and high heat transfer is associated with the thin boundary layer. Figure 5 presents conceptual views of the most notable characteristics of the rib induced secondary. As shown in Fig. 5a as the coolant near the surface of the channel passes over the rib, it separates from the surface. This separation results in relatively low heat transfer, due to a relatively hot cell being trapped in the area or recirculation. However, when the coolant reattaches to the surface (between two ribs), this is an area of relatively high heat transfer. This pattern of separation and recirculation continues through the channel with a pattern of repeating ribs. Ideal rib spacing is large enough for the coolant to reattach to the surface between the ribs (high heat transfer), but not so large that the boundary layer is allowed to develop freely, and the advantage of the thin boundary layer is lost. In addition to general flow separation and reattachment, the rib turbulators increase turbulent mixing. The relatively hot coolant near the surface is continuously mixing with the relatively cooler core coolant near the center of the channel. This mixing also serves to increase the heat transfer from the channel wall.

Ribs skewed to the mainstream flow are preferred to orthogonal ribs because they induce a second type of secondary flow. The coolant near the surface follows the angle of the rib. This angled rib induced secondary flow creates a set of counter-rotating vortices in the channel. The secondary flow follows the rib until it impinges on the side wall. After impingement on the side wall, the secondary induced flow returns to the other side wall, creating a vortex. This behavior is identical on both the leading and the trailing surfaces, so two counter-rotating vortices form in the channel.

Rib induced secondary flow obviously has a great impact on the heat transfer in the channel. Therefore, it is critical to optimize the rib configuration to take advantage of the rib induced secondary flow. For instance, rotating the turbulator, so it is not orthogonal to the mainstream flow significantly increases the heat transfer coefficients, due to the angled rib induced secondary flow. It has been shown that the ideal spacing for orthogonal ribs is approximately $P/e = 10$. As conceptually shown in Fig. 5a, with a spacing of 10, sufficient space is given between the ribs for reattachment of the flow between the

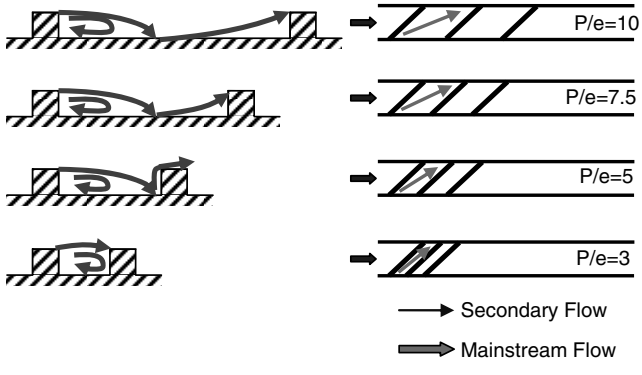

Fig. 5 Conceptual view of rib spacing effects on a) flow separation and reattachment and b) angled rib induced secondary flow.

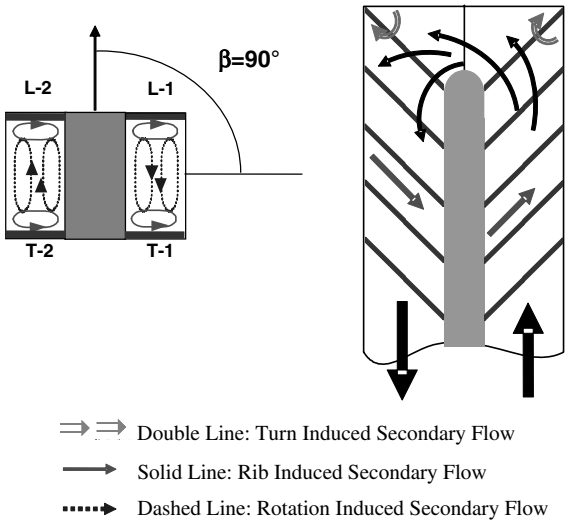

Fig. 6 Conceptual view of the mainstream flow and the secondary flow for the 45 deg angled ribs.

ribs, and this is also expected to be the case when the spacing decreases to 7.5. However, as the ribs continue to move closer together, the reattachment area becomes jeopardized. After separation, the coolant may impinge on the next downstream rib, or the coolant may completely pass over the next rib ($P/e = 3$), completely eliminating the desired flow behavior.

Because the ribs are skewed to the mainstream flow, regardless of how closely the ribs are spaced, the angled rib induced secondary flow is expected to be present, as shown in Fig. 5b. Unlike with 90 deg ribs, the coolant that is trapped between closely spaced angled ribs is expected to travel along the length of the ribs and create the counter-rotating vortices. Predictions from Su et al. [26] for a nonrotating channel with angled ribs ($P/e = 10$) show the angled rib induced, counter-rotating vortices are not limited to areas close to the rib-roughened walls; each vortex occupies nearly half of the channel cross section. If this trend is present, regardless of the rib spacing, the coolant between the ribs is moving (as opposed to being trapped), and additional heat transfer enhancement will occur.

A single pass channel with skewed turbulators introduces rib induced secondary flow that affects the level of heat transfer enhancement. In addition, the level of heat transfer enhancement is also altered by the addition of a second pass (connected to the first past via a 180 deg turn) and by rotation. Figure 6 shows the combined secondary flows induced by angled ribs, the 180 deg turn and rotation. Beginning with the secondary flow induced by rotation, the Coriolis force is known as the primary effect due to rotation. As conceptually shown in Fig. 6, with a 90 deg channel orientation, the Coriolis force induces a pair of vortices, which circulate toward the trailing wall for radial outward flow and toward the leading wall for radial inward flow. This cross-stream secondary flow pattern significantly increases heat transfer on the trailing wall in the first pass (radial outward flow) and the leading wall in the second pass (radial inward flow), but reduces heat transfer on the opposite walls (leading wall in the first pass and trailing wall in the second pass).

Therefore, rotation causes a difference in the heat transfer between the leading and the trailing walls. The effect of rotation is evaluated by the rotation number. The buoyancy parameter due to the centrifugal force and temperature difference is important because of the high rotating speed and large temperature difference in the actual engines. For the radial outward flow, the rotation induced buoyancy force aids the inertia force. This force opposes the inertia force in the second pass because the flow direction reversed. A buoyancy parameter, as defined by Wagner et al. [14], is used to present the combined effects of the Coriolis and buoyancy forces:

$$Ro = \frac{\Omega D_h}{V} \tag{7}$$

$$Bo_x = \left(\frac{\Delta\rho}{\rho}\right)_x (Ro)^2 \frac{R_x}{D_h} \tag{8}$$

This local buoyancy parameter can be rewritten by incorporating the measured wall and coolant temperatures as shown in Eq. (9):

$$Bo_x = \frac{T_{w,x} - T_{b,x}}{T_{f,x}} (Ro)^2 \frac{R_x}{D_h} \tag{9}$$

The local film temperature is the average of the local wall and the local coolant temperatures.

$$T_{f,x} = (T_{w,x} + T_{b,x})/2 \tag{10}$$

When the flow passes through the 180 deg turn, the flow impinges on the outer wall due to the centrifugal force, then reattaches on the inner wall in the second pass. It creates a circulation zone right after the turn near the inner wall in the second pass. Two additional circulation zones occur in the outer corners of the turn because of the geometry. These flow structures, due to the turn, result in different heat transfer enhancements inside the turn and after the turn.

All of these secondary flows, induced by angled ribs, the 180 deg turn, and rotation, interact to make flow through a rib-roughened serpentine passage very complex. The combination of these flows may result in further enhancement of the heat transfer, or they may have a negative impact on the heat transfer trend. The following discussion of the experimental results will offer complimentary proof to the conceptual view of the combined effects of secondary flows.

Regionally Averaged Heat Transfer Distributions

$P/e = 10$

To quantify the heat transfer enhancement in the various rib-roughened channel, the regionally averaged Nusselt number ratios are presented based on the smooth area of the cooling passage; this definition will show the actual heat transfer enhancement compared to a smooth, nonrotating channel. Figure 7 shows the regionally averaged Nusselt number ratios in nonrotating and rotating channels with a rib spacing of $P/e = 10$. This rib spacing is considered the baseline case, as the spacing has been selected by many research groups as the "optimum spacing" based on previous nonrotating results, with orthogonal ribs.

From the stationary data in Fig. 7, it is clear that the greatest heat transfer enhancement occurs at the lowest Reynolds number of 5000. As the Reynolds number increases, the heat transfer coefficients increase, but the Nusselt number ratios decrease, as the Dittus-Boelter/McAdams correlation absorbs the effect of the Reynolds number. The general trend for all four Reynolds numbers considered is relatively uniform heat transfer enhancement in the first pass, a rise in the Nusselt number ratios in the turn followed by a decrease leaving the turn, and again uniform enhancement through the second pass, with approximately the same level of enhancement in both the first and second passes of the cooling channel.

The effect of rotation is clearly shown in the first passage of the cooling channel by both the additional enhancement of the heat transfer on the trailing surface at the expense of reduced heat transfer on the leading surface. The declination of the Nusselt number ratio on the leading surface is more significant than the heat transfer enhancement; this can be explained from two vantage points, but is more likely a combination of the two. First, it is expected that the heat transfer coefficients on the leading surface will decrease, as the coolant is forced away from the leading surface due to the rotation induced Coriolis force; however, the dramatic decrease shown for the current 1:2 ribbed channel has not been observed in large aspect ratio channels (1:1, 2:1, or 4:1). Numerical predictions by Su et al. [26] showed a destructive interaction between the rotation induced and angled rib induced flow near the leading surface. The vortices induced by the angled ribs and rotation interact, and a small pocket of hot air becomes trapped near the leading surface. The interaction with the core of the mainstream coolant is minimized, and the heat

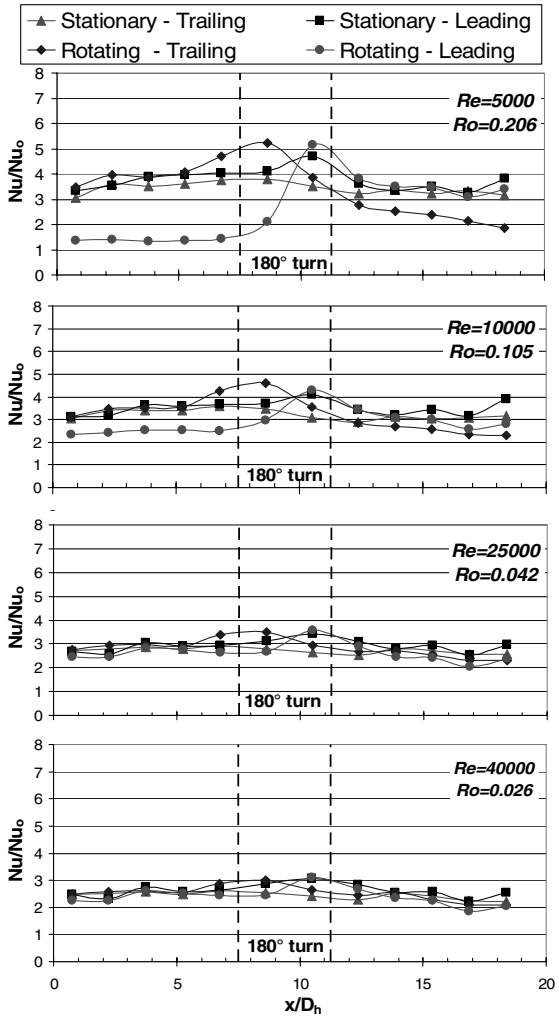

Fig. 7 Nusselt number ratio in the $AR = 1{:}2$ channel with $P/e = 10$ based on a smooth area.

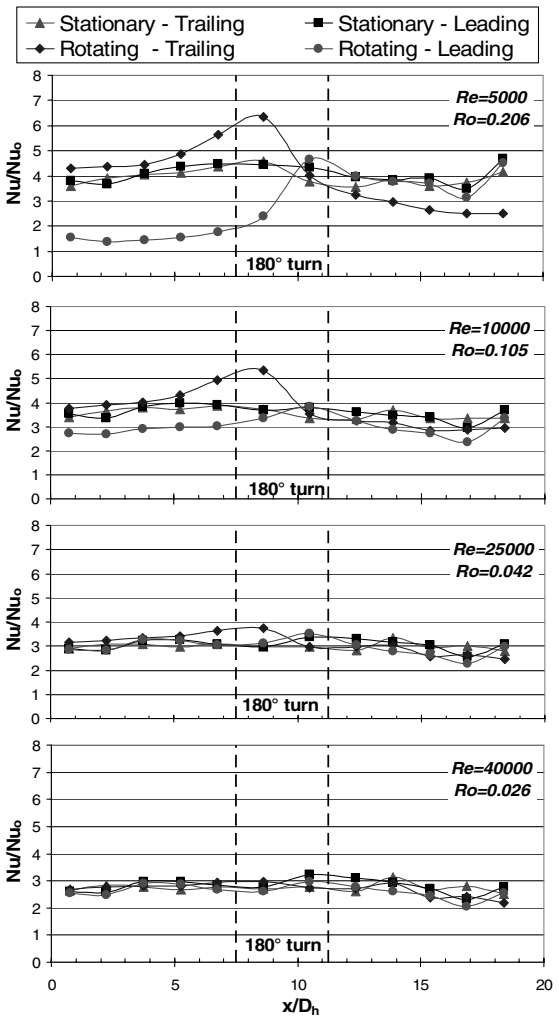

Fig. 8 Nusselt number ratio in the $AR = 1{:}2$ channel with $P/e = 7.5$ based on a smooth area.

transfer coefficients are dramatically reduced because the relatively warm air is trapped near the surface. Secondly, the enhancement on the trailing surface is not equal to the declination on the leading surface because the heat transfer enhancement on the trailing surface is relatively high, due to the rib enhancement. Although the Coriolis force pushes the core of the coolant to the trailing edge, this additional enhancement due to rotation is minimal.

The effect of rotation is seen in the second pass most apparently by the declination of the heat transfer coefficients on the trailing surface. As shown in previous studies, the rotation induced buoyancy force opposes the rotation induced Coriolis force. Unlike in the first pass, where these two rotation induced forces work together, the opposition of the forces results in a reduced effect of rotation in the second pass. Therefore, the difference between the Nusselt number ratios on the leading and trailing surfaces decreases.

Because the rotation speed and the hydraulic diameter of the channel remain constant, the rotation number varies inversely with the mean coolant velocity through the channel, and likewise with the Reynolds number of the coolant (increasing the Reynolds number decreases the rotation number). As the Reynolds number increases, the effect of rotation clearly diminishes, as the rotation number begins to approach zero, and minimal variation occurs between the stationary and rotating data at $Re = 40,000$ ($Ro = 0.026$).

$P/e = 7.5$

The rib pitch-to-height ratio is reduced to 7.5 to compare the heat transfer enhancement in both stationary and rotating channels to similar channels with $P/e = 10$. As shown in Fig. 8, the general trends for the heat transfer enhancement in cooling channels with $P/e = 7.5$ are similar to those with $P/e = 10$. However, the level of heat transfer enhancement for the nonrotating channel with a rib spacing of 7.5 is greater than the nonrotating channel with the rib spacing of 10. Attention must be directed to the calculation of the heat transfer coefficient; the regionally averaged results are based on the smooth channel area. As noted in Table 1, when $P/e = 10$, the ribs increase the heat transfer area by 26.5%; however, with $P/e = 7.5$, the heat transfer area is increased by 35.3%. The rise in the Nusselt number ratios from the rib spacing of 10 to 7.5 can be attributed to the increased heat transfer area.

The effect of rotation is most apparently seen at the lowest Reynolds number of 5000 ($Ro = 0.2$). The clear enhancement of heat transfer on the trailing surface and reduction on the leading surface are again seen in the first pass. The effect of rotation is again reduced in the second pass, with no substantial enhancement to the leading surface.

$P/e = 5$

The Nusselt number ratios for the rib spacing of 5 are shown in Fig. 9. The heat transfer enhancements in this nonrotating ribbed channel are significantly higher than those in the previous two channels ($P/e = 7.5$ and 10). The heat transfer area has increased to twice that in the channel with $P/e = 10$ and 1.5 times the area in the channel with $P/e = 7.5$. The enhancement in this nonrotating channel with $P/e = 5$ can be almost 6 times greater than the enhancement in a nonrotating channel without rib turbulators. As with the previous channels, the effect of rotation is most clearly seen

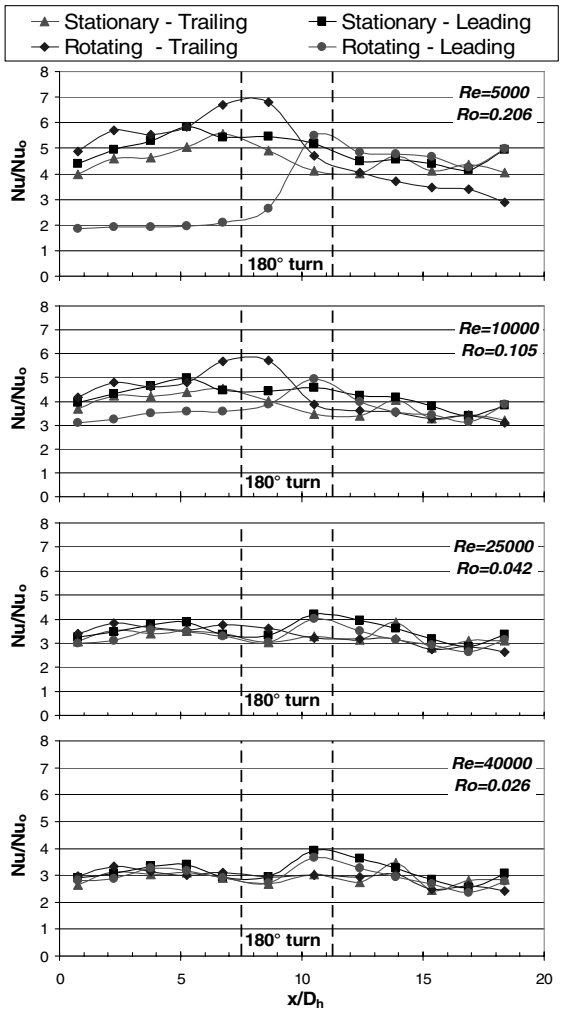

Fig. 9 Nusselt number ratio in the $AR = 1{:}2$ channel with $P/e = 5$ based on a smooth area.

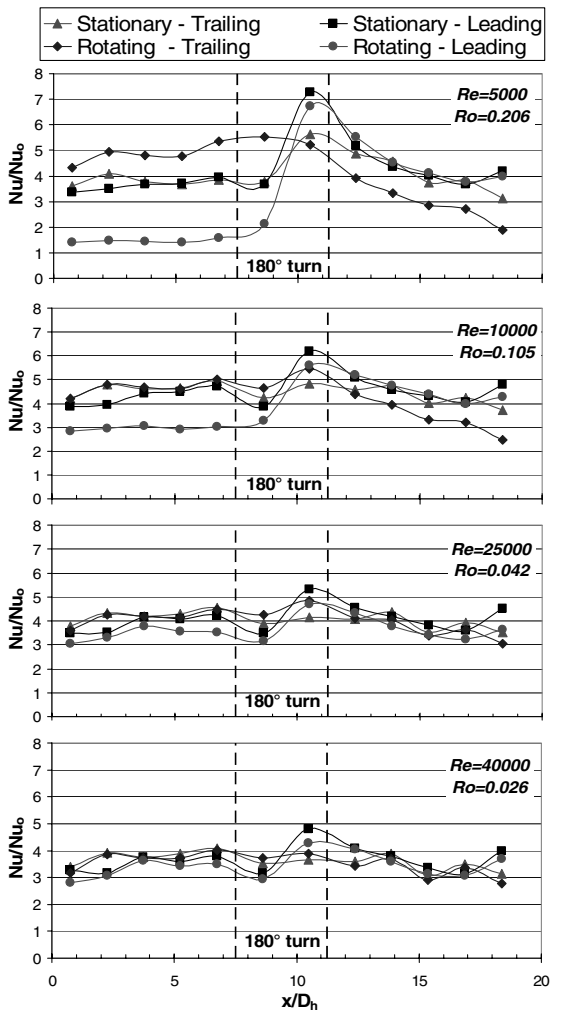

Fig. 10 Nusselt number ratio in the $AR = 1{:}2$ channel with $P/e = 3$ based on a smooth area.

at $Re = 5000$ by the enhancement of the heat transfer coefficients on the trailing surface and the reduction on the leading surface. Similar to $P/e = 7.5$, the effect of rotation in the second pass is seen by the decreased heat transfer coefficients on the trailing surface, with no significant enhancement due to rotation to the leading surface (in the second pass). As the rotation number decreases, the effect of rotation decreases the heat transfer enhancement on both the leading and trailing surfaces, and the Nusselt number ratios in rotating channel converge to the nonrotating data.

$P/e = 3$

The regionally averaged heat transfer enhancement for the final rib spacing of 3 is shown in Fig. 10. At the higher Reynolds numbers, the level of heat transfer enhancement in the nonrotating channels is greater than the previously mentioned channels. However, at the lowest Reynolds number of 5000, the heat transfer enhancement is less than with the previous case of $P/e = 5$. The continued rise in the heat transfer enhancement is unexpected based on the previous rib spacing studies with 90 deg ribs. Previous studies indicate the optimum rib spacing occurs for P/e ratios ranging from 7.5 to 10. However, the 45 deg angled ribs with the smallest spacing of 3 generally give the greatest heat transfer enhancement ($Re > 10,000$).

The heat transfer area has now increased 88.3% over the smooth area. Channels with orthogonal ribs would also see a similar area increase, but the heat transfer enhancement does not continue to rise, as seen with these skewed ribs. Referring back to Fig. 5a, it was shown that hot coolant is trapped between two ribs that are closely spaced, and the coolant has the tendency to pass over the top of the ribs, without boundary layer redevelopment between the ribs. However, with the angled ribs, the coolant between the skewed ribs is expected to follow the rib until impinging on the side wall (Fig. 5b), where it turns, creating a vortex. The circulation allows this coolant, which would become stagnant in the channel with 90 deg ribs, to mix with the mainstream, and therefore, increase the heat transfer coefficients on the ribbed wall. The circulation of this coolant combined with the increased area results in the best heat transfer enhancement of the four rib spacings considered.

The general effect of rotation seen in the other channels is apparent in this channel with the closely spaced ribs. However, as the rib spacing decreases, the effect of rotation increases. With a rib spacing of unity, two adjacent ribs would be side by side, and the channel would be smooth. As P/e decreases, the effect of rotation increases, as if the channel were becoming a smooth channel. A general finding of rotating channels with any type of turbulators is that the addition of turbulators weakens the effect of rotation. However, with the addition of more ribs in the present study, the effect of rotation is becoming stronger. This can be explained because with the spacing between the ribs decreasing, the channel is taking on attributes of a smooth channel. In addition, with the number of ribs increasing, the rib induced secondary flow may be weakened, and therefore, the impact of the rotation induced secondary flow is more apparent.

Averaged Nusselt Number Ratio: Nonrotating Channel

The channel averaged Nusselt number ratios for the nonrotating channels are shown in Fig. 11. The first-pass channel averaged data,

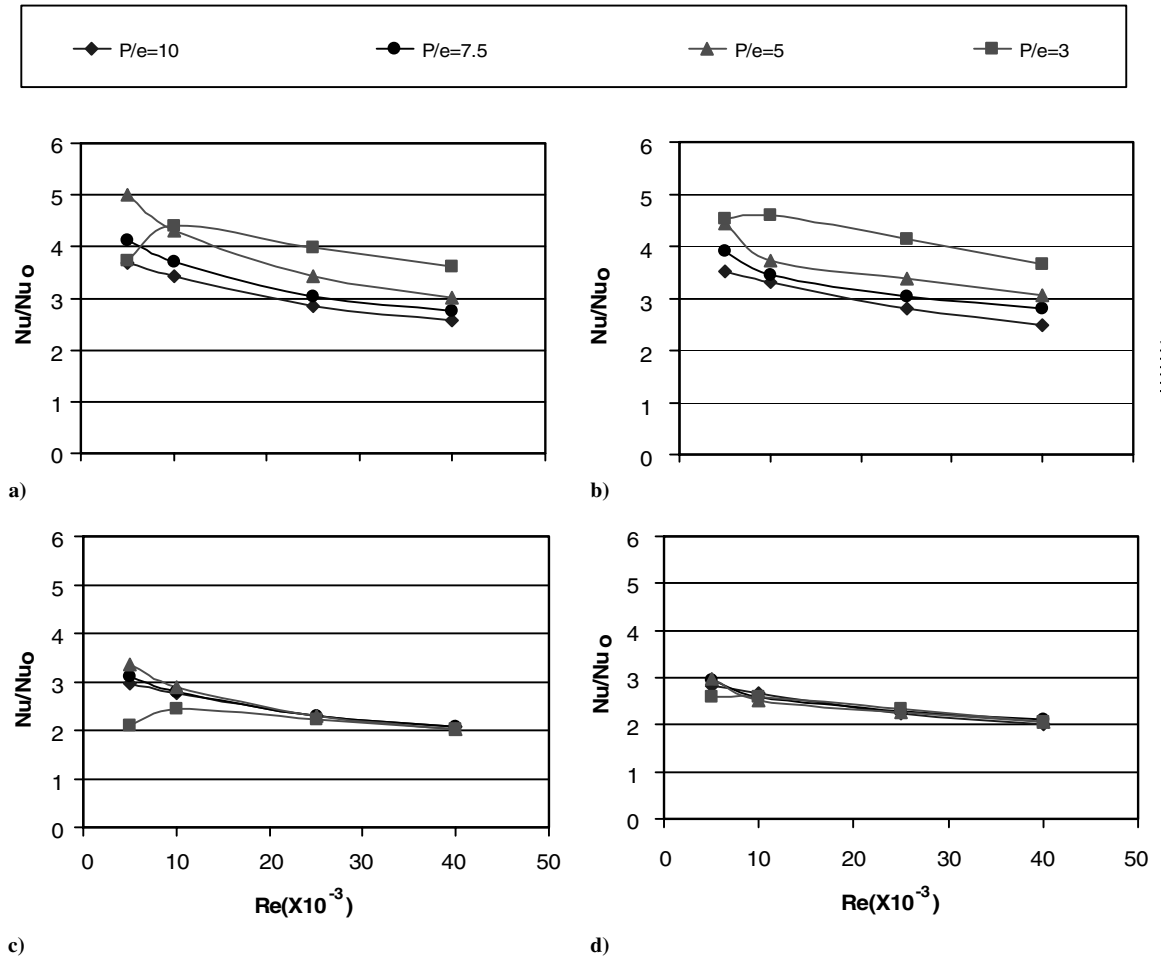

Fig. 11 Average Nusselt number for the a) first pass (smooth area); b) second pass (smooth area); c) first pass (total area); and d) second pass (total area) in the stationary channel.

as shown in Fig. 11a, are the average of the leading and the trailing surfaces in the first pass. Similarly, the second-pass channel average, as shown in Fig. 11b, includes all regions on the leading and the trailing surfaces in the second pass. Figures 11c and 11d correspond to Figs. 11a and 11b with the effect of the increased area being taken into account. It is clearly shown that the channel averaged heat transfer increases with the decreasing P/e ratio, if the smooth area is applied to obtain the heat transfer coefficients. The $P/e = 3$ case has the highest channel averaged Nusselt number ratio ($Re \geq 10,000$). The level of heat transfer in the first pass is slightly higher than the second pass. However, if the total area is applied (11c and 11d), the curves for all four rib spacings generally merge together. If the rib area is considered when calculating the heat transfer coefficients, the benefit of the additional ribs is eliminated. As the rib induced secondary flow is different for the various rib pitches, it would be expected that the heat transfer coefficients based on the total heat transfer area would vary for the different rib pitches. With orthogonal turbulators, the heat transfer enhancement is driven by the separation and reattachment of the coolant near the wall. However, with the ribs angled to the mainstream flow, the heat transfer enhancement is driven by the combined effect of flow separation and reattachment with the rib induced vortices as the coolant follows the ribs from the inner wall to the outer wall. Unlike with 90 deg ribs, where decreasing the pitch of the ribs decreases the heat transfer coefficients (with the inclusion of the total heat transfer area), the rib induced secondary flow combined with the changing heat transfer area yields the same level of heat transfer enhancement for all rib spacings.

Because a number of studies are available for nonrotating data, it is worthwhile to compare the nonrotating results of the current study to those of previous studies. Because the studies that consider the effect of rib spacing are done in single pass test sections, the Nusselt numbers on the leading and trailing surfaces for regions 1–5 are averaged to give the first-pass average with minimal influence of the 180 deg turn. As shown in Fig. 12, Han [5,6] experimentally determined the maximum heat transfer enhancement occurs for $P/e = 10$ for orthogonal ribs (based on the smooth channel area). However, the current study with skewed ribs refutes this finding, with the heat transfer enhancement continuing to rise as P/e decreases. Because the ribs are skewed to the mainstream flow, the coolant does not become trapped between two ribs. This angled rib induced secondary flow obviously benefits the heat transfer enhancement, and closely spaced, skewed ribs offer the best heat transfer enhancement.

Averaged Nusselt Number Ratio: Rotating Channel

The average Nusselt number ratios for the rotating channels are shown in Fig. 13. Similar to Fig. 11, the averages are grouped according to first or second pass and heat transfer enhancement based on smooth or total areas. Unlike the previous figure, the leading and trailing surfaces are not averaged together, as it is interesting to see the effect of rotation. From Fig. 13a the effect of rotation is clear with the enhancement of the heat transfer on the trailing surfaces. At the lowest Reynolds numbers of 5000 and 10,000, the trailing surface of the channel with $P/e = 5$ has the greatest heat transfer enhancement; however, when the Reynolds number increases, the trailing surface in the channel with $P/e = 3$ has the greatest Nusselt numbers. However, the first pass of the channel with $P/e = 10$ is most adversely affected by rotation. Figure 13b compares the effect of rotation in the second passes of the channels with various rib spacings. The cooling channel with the ribs spaced closely together ($P/e = 3$) has greater heat transfer enhancement than the other cooling channels. As expected, the effect of rotation is less evident in

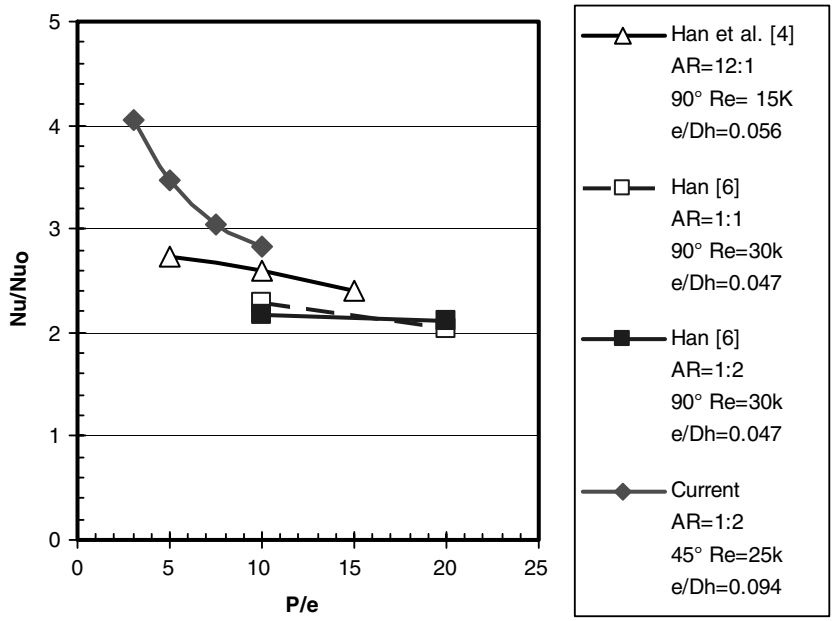

Fig. 12 Effect of rib spacing on heat transfer enhancement in cooling channels with various aspect ratios and rib spacings.

the second pass of the channel, than the first pass. Similar to the nonrotating channels (Fig. 11), with the inclusion of the total heat transfer area the Nusselt number ratio variation between the channels decreases. However, the effect of rotation remains seen in the first pass with the separation between the leading and trailing surfaces at the lower Reynolds numbers (higher rotation numbers). In the second pass, where the effect of rotation is lessened, the heat transfer enhancement for both the leading and trailing surfaces of all the

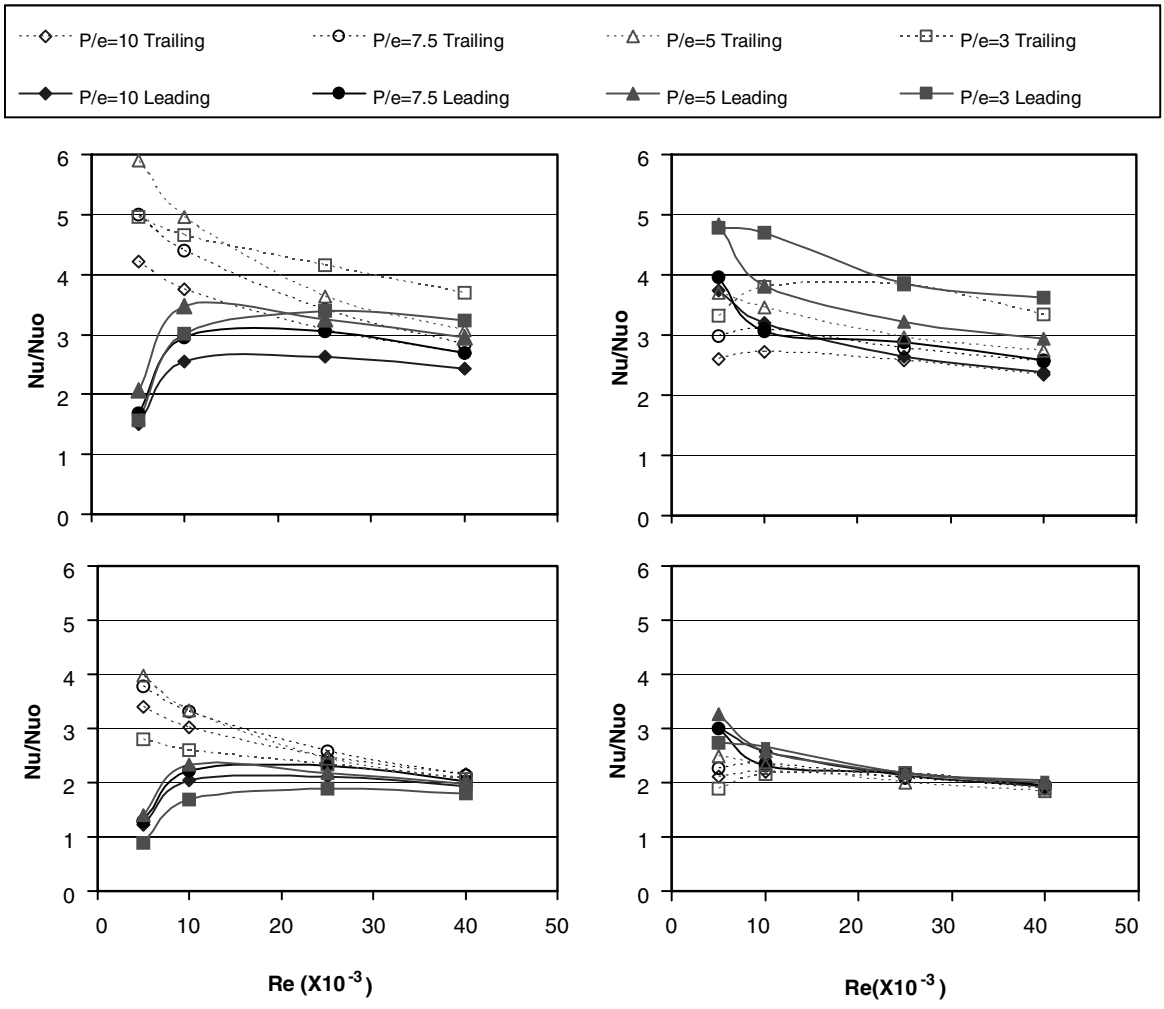

Fig. 13 Average Nusselt number for the a) first pass (smooth area); b) second pass (smooth area); c) first pass (total area); and d) second pass (total area) in the rotating channel.

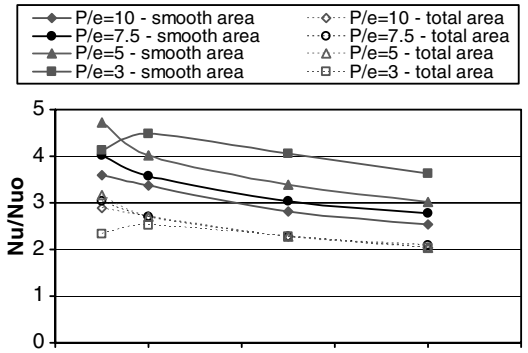

a) Channel average heat transfer - stationary

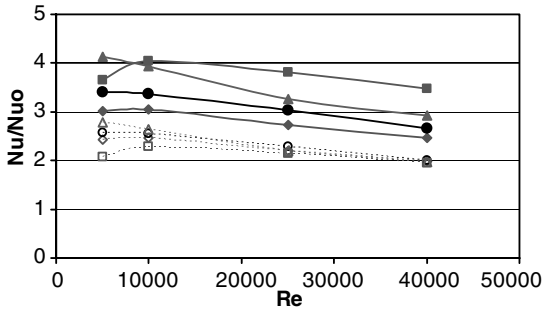

b) Channel average heat transfer - rotating

Fig. 14 Channel averaged Nusselt number ratio for the a) stationary case and b) rotating case for the entire channel.

channels converge together with increasing Reynolds number (decreasing rotation number).

Thermal Performance

The heat transfer enhancement must be evaluated against the pressure penalty for each case to determine the best rib spacing. One way to evaluate the rib performance is to calculate the thermal performance for a given rib spacing. The definition of thermal performance has been defined in Eq. (6).

The overall channel averaged Nusselt number ratio is obtained by averaging the leading and trailing surfaces of every region, so 24 regions are included in the average. The channel averaged Nusselt number ratios are shown in Fig. 14. The overall channel averaged Nusselt number increases with the decreasing P/e ratio for both nonrotating and rotating channels. As the Reynolds number increases, the Nusselt number ratio decreases. However, if the total area is applied, $P/e = 3$ has the lowest overall channel averaged Nusselt number ratio for both the nonrotating and rotating channels, at the lower Reynolds numbers of 5000 and 10,000. When considering the heat transfer enhancement based on the total area, as the Reynolds number increases, all four channels have the same level of heat transfer enhancement, as the advantage of the increased heat transfer area is removed.

The pressure penalty is presented in terms of the friction factor ratio. The friction factor ratio for both the nonrotating and rotating channels is shown in Fig. 15. The pressure drop inside a ribbed channel is higher than the smooth channel because the rib trips the flow and produces more losses. As more ribs are added to the surface, more flow is tripped and the pressure drop increases. However, when the rib spacing decreases to a minimum, the flow will mostly pass over the ribs. In this case, the flow behavior is similar to the smooth channel and pressure drop decreases. The friction factor ratio increases with decreasing P/e ratio down to $P/e = 5$ for both nonrotating and rotating cases. As the spacing decreases below 5, the friction factor ratios begin to decrease. In general, the pressure penalty is greater for the nonrotating case. As the Reynolds number increases, the friction factor ratio also increases.

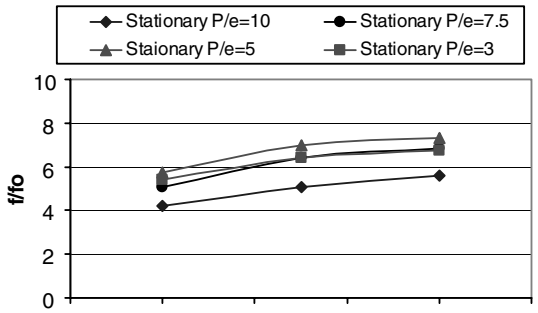

a) Friction factor ratio - stationary

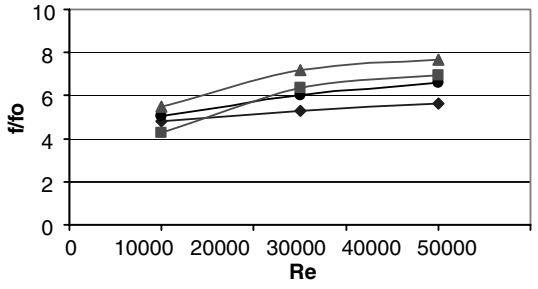

b) Friction factor ratio - rotating

Fig. 15 Overall friction factor ratios for the a) stationary case and b) rotating case.

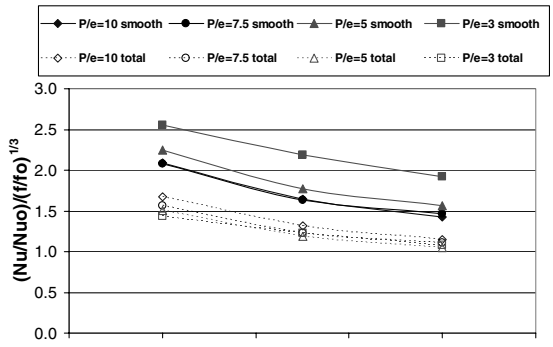

a) Stationary thermal performance

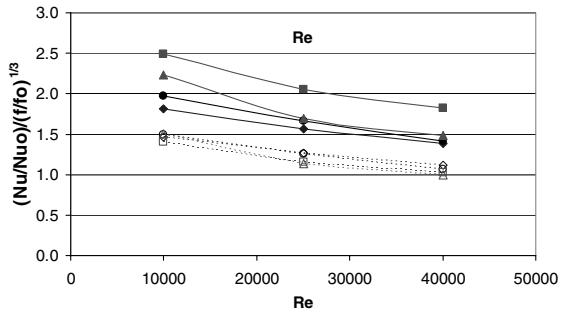

b) Rotating thermal performance

Fig. 16 Thermal performance for the a) stationary case and b) rotating case.

The overall thermal performance for both nonrotating and rotating channels is shown in Fig. 16. It is obvious that the $P/e = 3$ case has the best thermal performance for both stationary and rotating channels. With the heat transfer enhancement based on the smooth area, the spacing of $P/e = 3$ has the greatest heat transfer enhancement primarily due to the increased heat transfer area. The thermal performance decreases with increasing P/e ratio. However, for the total heat transfer area, $P/e = 10$ gives the best overall

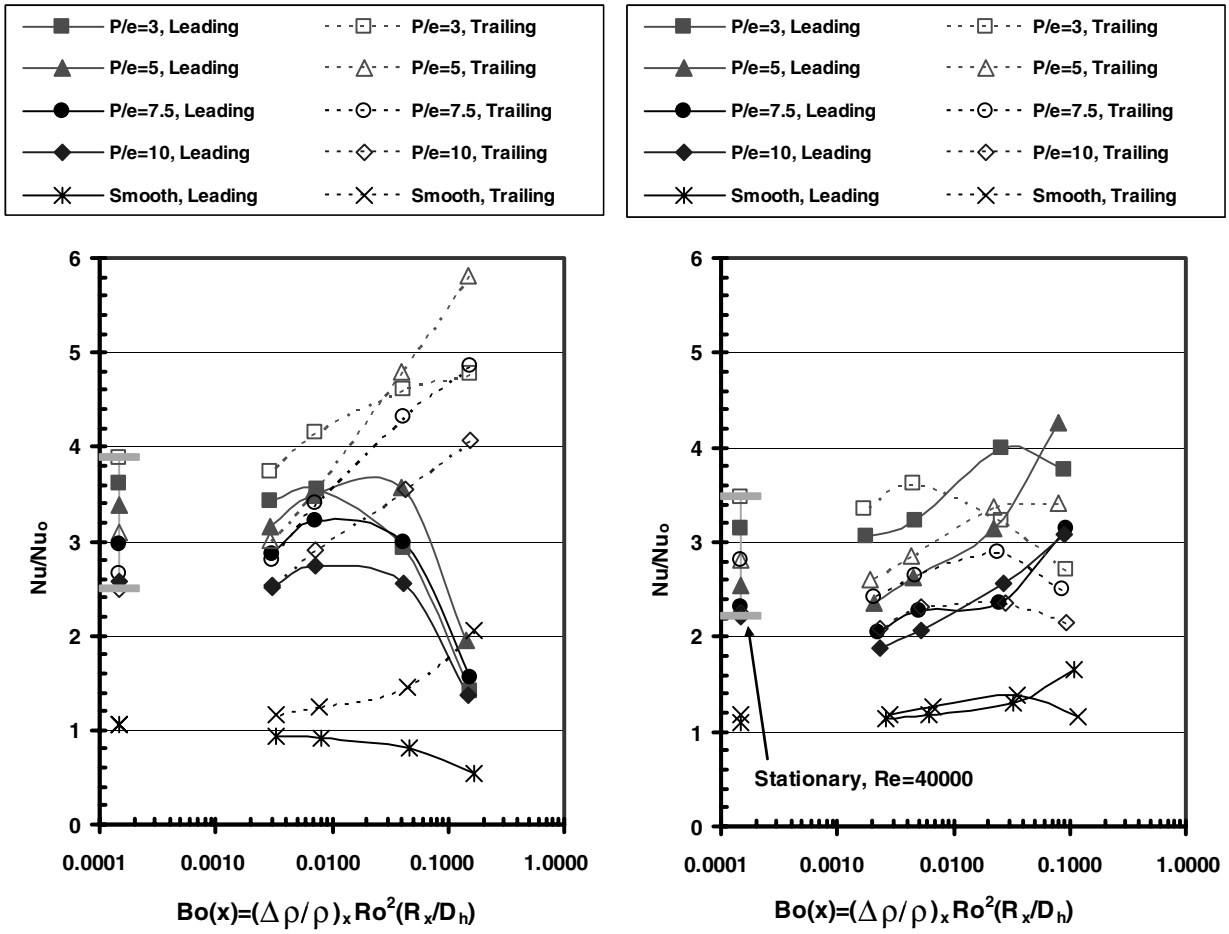

a) Leading and Trailing, #4 b) Leading & Trailing, #11

Fig. 17 Nusselt number ratio comparison with buoyancy effects in regions 4 and 11.

thermal performance due to the decreased pressure losses, and this is true for both rotating and nonrotating channels.

Regional Buoyancy Effect on Heat Transfer Enhancement

In addition to considering the overall thermal performance of the different rib spacings, it is worthwhile to know how each channel is affected by the local buoyancy parameter. Figures 17 and 18 show the Nusselt number ratios as a function of the local buoyancy parameter. The regions considered for the comparison are region 4 (first pass, fully developed), region 11 (second pass, fully developed), region 6 (first pass, turn), and region 7 (second pass, turn). Each of these regions, as shown in Fig. 3, offer interesting comparisons for the combined effect of density ratio, rotation number, Reynolds number, and buoyancy. Therefore, the effect of rotation and pitch can be easily compared on the leading and trailing surfaces of the cooling channel. The Nusselt number ratios plotted in these two figures are based on the smooth channel area, and the Nusselt number ratios from smooth channels are added as a reference from Fu et al. [22].

Figure 17 shows the heat transfer enhancement on the trailing surfaces for the rib spacings of 7.5 and 10 increases at the same rate at region 4. Although the heat transfer coefficients on the trailing surface in the channel with $P/e = 10$ gradually rise, this channel has the least enhancement. The spacings of $P/e = 3$ and 5 produced the greatest heat transfer enhancement on the trailing surface at the low and high buoyancy parameters, respectively. The effect of the buoyancy parameter on the heat transfer enhancement along the leading surface is interesting for all four rib spacings. As the buoyancy parameter increases from 0.0013 to 0.014, the Nusselt number ratios remain uniform, and beyond $Bo_x = 0.014$, the Nusselt number ratios decrease dramatically.

The effect of rotation in the first pass is compared to the effect of rotation in the second pass by comparing Figs. 17a and 17b. As expected, the Nusselt number ratios on the leading surface are increasing with the increasing buoyancy parameter for all rib spacings, whereas the trailing surfaces only see the expected declination in heat transfer at the maximum buoyancy parameter.

In addition to considering the fully developed regions of the channel, the turn region is always of prime concern for turbine designers. Figure 18 compares the Nusselt number ratios on the leading and trailing surfaces on regions 6 and 7, inside the 180 deg turn. The general heat transfer trends at region 6 are the same as those for region 4. The trailing surfaces experience heat transfer enhancement, while the heat transfer coefficients on the leading surface decrease. However, the level of enhancement on the trailing surface for all rib configurations considered is much greater at region 6 than region 4. Unlike region 11, the heat transfers on both the leading and trailing surfaces at region 7 increase with the increasing buoyancy parameter. Although the heat transfer enhancement on the leading surfaces is generally greater than for the trailing surfaces.

Interestingly, in the first pass (regions 4 and 6) the rib spacings of $P/e = 3$ give the greatest heat transfer enhancement at the higher buoyancy parameters: the greatest heat transfer enhancement on the trailing surface with the least reduction on the leading surface. However, in the second pass of the ribbed channels, $P/e = 5$ tends to be the preferred rib spacing.

Conclusions

This study investigated the rib spacing effect in a rotating two-pass rectangular channel with an aspect ratio of 1:2. The channel is roughened by placing 45 deg angled ribs on the leading and trailing

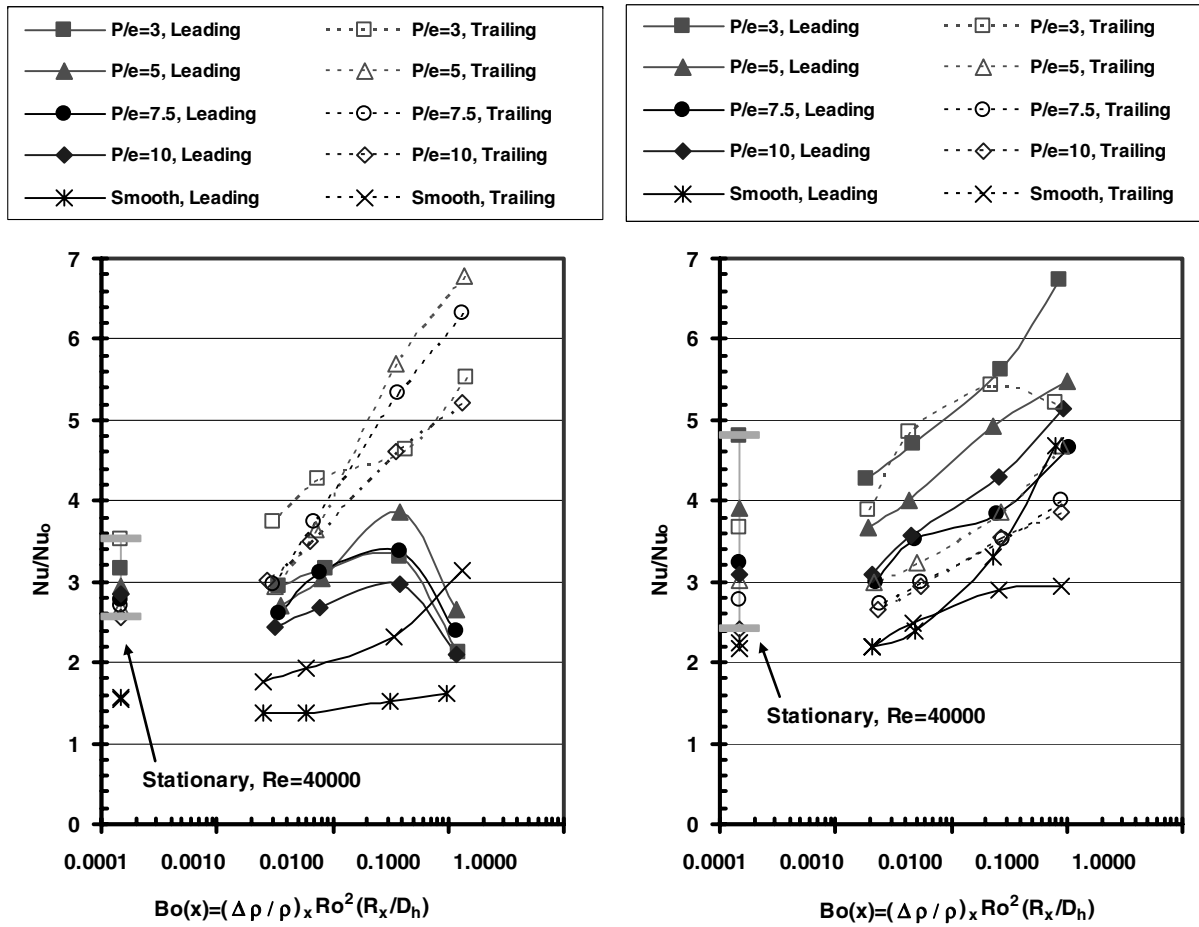

a) Leading & Trailing, #6 b) Leading & Trailing, #7

Fig. 18 Nusselt number ratio comparison with buoyancy effects in regions 6 and 7.

surfaces. The rotating speed was fixed at 550 rpm for all cases while the Reynolds number varied from 5000 to 40,000. The change in rotation number is dependent on the changing Reynolds number and ranges from 0.2–0.026. Based on the discussion, the main conclusions are as follows:

1) The rotation effect increased heat transfer on the trailing surface but decreased the heat transfer on the leading surface in the first pass. In the second pass, the difference of the heat transfer between the leading and trailing surfaces was reduced under the rotating condition when compared to the first pass. The effect of rotation was most clearly seen by the declination of the Nusselt number ratios on the leading surface of the first pass.

2) Based on the smooth heat transfer area, the $P/e = 3$ case obtains the best thermal performance for both rotating and nonrotating channels in the present study. This finding cannot be extended to cooling channels with orthogonal ribs. The secondary flow induced by the skewed ribs forces the coolant between two ribs to circulate (unlike when the fluid is simply trapped between two orthogonal ribs), and thus the level of heat transfer enhancement continues to rise as the P/e ratio decreases for channels with angled ribs.

3) When considering the heat transfer enhancement based on the smooth channel area, the Nusselt number ratios increase as P/e decreases. However, if calculation of the heat transfer coefficient is based on the total heat transfer area, all four rib spacings offer comparable levels of heat transfer enhancement. Including the total heat transfer area eliminates the advantage of the increased area from the addition of more ribs.

4) The friction factor increases with the decreasing P/e ratio for the P/e ratio down to 5. The $P/e = 5$ case has the highest pressure penalty for both rotating and nonrotating channels. As the P/e ratio further decreases to 3, the friction factor reduces.

References

[1] Han, J. C., Dutta, S., and Ekkad, S. V., *Gas Turbine Heat Transfer and Cooling Technology*, Taylor and Francis, New York, 2000.

[2] Han, J. C., and Park, J. S., "Developing Heat Transfer in Rectangular Channels with Rib Turbulators," *International Journal of Heat and Mass Transfer*, Vol. 31, Jan. 1988, pp. 183–195.

[3] Park, J. S., Han, J. C., Huang, Y., and Ou, S., "Heat Transfer Performance Comparisons of Five Different Rectangular Channels with Parallel Angled Ribs," *International Journal of Heat and Mass Transfer*, Vol. 35, No. 11, 1992, pp. 2891–2903.

[4] Han, J. C., Glicksman, L. R., and Rohsenow, W. M., "An Investigation of Heat Transfer and Friction for Rib-Roughened Surfaces," *International Journal of Heat and Mass Transfer*, Vol. 21, Aug. 1978, pp. 1143–1156.

[5] Han, J. C., "Heat Transfer and Friction in Channels with Two Opposite Rib-Roughened Walls," *ASME Journal of Heat Transfer*, Vol. 106, Nov. 1984, pp. 774–781.

[6] Han, J. C., "Heat Transfer and Friction Characteristics in Rectangular Channels with Rib Turbulators," *ASME Journal of Heat Transfer*, Vol. 110, May 1988, pp. 321–328.

[7] Taslim, M. E., and Wadsworth, C. M., "An Experimental Investigation of the Rib Surface-Averaged Heat Transfer Coefficient in a Rib-Roughened Square Passage," *ASME Journal of Turbomachinery*, Vol. 119, April 1997, pp. 381–389.

[8] Taslim, M. E., and Lengkong, A., "45 deg Staggered Rib Heat Transfer Coefficient Measurements in a Square Channel," *ASME Journal of Turbomachinery*, Vol. 120, July 1998, pp. 571–580.

[9] Taslim, M. E., and Korotky, G. J., "Low-Aspect-Ratio Rib Heat Transfer Coefficient Measurements in a Square Channel," *ASME Journal of Turbomachinery*, Vol. 120, Oct. 1998, pp. 831–838.

[10] Rau, G., Cakan, M., Moeller, D., and Arts, T., "The Effects of Periodic Ribs on the Local Aerodynamic and Heat Transfer Performance of a Straight Cooling Channel," *ASME Journal of Turbomachinery*, Vol. 120, April 1998, pp. 368–375.

[11] Astarita, T., and Cardone, G., "Convective Heat Transfer in a Square Channel with Angled Ribs on Two Opposite Walls," *Experiments in Fluids*, Vol. 34, April 2003, pp. 625–634.
[12] Taslim, M. E., and Spring, S. D., "Effects of Turbulator Profile and Spacing on Heat Transfer and Friction in a Channel," *Journal of Thermophysics and Heat Transfer*, Vol. 8, No. 3, 1994, pp. 555–562.
[13] Bailey, J. C., and Bunker, R. S., "Heat Transfer and Friction in Channels with Very High Blockage 45° Staggered Turbulators," ASME Paper GT 2003-38611, June 2003.
[14] Wagner, J. H., Johnson, B. V., and Hajek, T. J., "Heat Transfer in Rotating Passage with Smooth Walls and Radial Outward Flow," *ASME Journal of Turbomachinery*, Vol. 113, Jan. 1991, pp. 42–51.
[15] Wagner, J. H., Johnson, B. V., and Kooper, F. C., "Heat Transfer in Rotating Passage with Smooth Walls," *ASME Journal of Turbomachinery*, Vol. 113, July 1991, pp. 321–330.
[16] Johnson, B. V., Wagner, J. H., Steuber, G. D., and Yeh, F. C., "Heat Transfer in Rotating Serpentine Passages with Trips Skewed to the Flow," *ASME Journal of Turbomachinery*, Vol. 116, Jan. 1994, pp. 113–123.
[17] Dutta, S., and Han, J. C., "Local Heat Transfer in Rotating Smooth and Ribbed Two-Pass Square Channels with Three Channel Orientations," *ASME Journal of Heat Transfer*, Vol. 118, Aug. 1996, pp. 578–584.
[18] Al-Hadhrami, L., and Han, J. C., "Effect of Rotation on Heat Transfer in Two-Pass Square Channels with Five Different Orientations of 45° Angled Rib Turbulators," *International Journal of Heat and Mass Transfer*, Vol. 46, Feb. 2003, pp. 653–669.
[19] Fu, W. L., Wright, L. M., and Han, J. C., "Heat Transfer in Two-Pass Rotating Rectangular Channels (AR = 2:1) with Discrete V-Shaped and Discrete Angled Rib Turbulators," ASME Paper IMECE2004-50563, 2004.
[20] Griffith, T. S., Al-Hadhrami, L., and Han, J. C., "Heat Transfer in Rotating Rectangular Cooling Channels (AR = 4) with Angled Ribs," *ASME Journal of Heat Transfer*, Vol. 124, Aug. 2002, pp. 617–625.
[21] Wright, L. M., Fu, W. L., and Han, J. C., "Thermal Performance of Angled, V-Shaped, and W-Shaped Rib Turbulators in Rotating Rectangular Cooling Channels (AR = 4:1)," ASME Paper GT2004-54073, June 2004.
[22] Fu, W. L., Wright, L. M., and Han, J. C., "Buoyancy Effects on Heat Transfer in Five Different Aspect-Ratio Rectangular Channels with Smooth Walls and 45-Degree Ribbed Walls," ASME Paper GT 2005-68493, May 2005.
[23] Taslim, M. E., Rahman, A., and Spring, S. D., "An Experimental Investigation of Heat Transfer Coefficients in a Spanwise Rotating Channel with Two Opposite Rib-Roughened Walls," *ASME Journal of Turbomachinery*, Vol. 113, Jan. 1991, pp. 75–82.
[24] Taslim, M. E., Bondi, L. A., and Kercher, D. M., "An Experimental Investigation of Heat Transfer in an Orthogonally Rotating Channel Roughened with 45 deg Criss-Cross Ribs on Two Opposite Walls," *ASME Journal of Turbomachinery*, Vol. 113, July 1991, pp. 346–353.
[25] Kline, S. J., and McClintock, F. A., "Describing Uncertainty in Single-Sample Experiments," *Mechanical Engineering*, Vol. 75, Jan. 1953, pp. 3–8.
[26] Su, G., Chen, H. C., Han, J. C., and Heidmann, D., "Computation of Flow and Heat Transfer in Two-Pass Rotating Rectangular Channels (AR = 1:1, AR = 1:2, AR = 1:4) with 45-Deg Angled Ribs by a Reynolds Stress Turbulence Model," ASME Paper GT2004-53662, June 2004.